Metrol. Meas. Syst., Vol. XX (2013), No. 4, pp. 601–612.

PAN POLSKA AKADEMIA NAUK

METROLOGY AND MEASUREMENT SYSTEMS

Index 330930, ISSN 0860-8229
www.metrology.pg.gda.pl

M&MS

CORRECTION OF THE REFRACTION PHENOMENON IN PHOTOGRAMMETRIC MEASUREMENT SYSTEMS

David Samper, Jorge Santolaria, Ana Cristina Majarena, Juan José Aguilar

Universidad de Zaragoza, Department of Design and Manufacturing Engineering, Torres Quevedo Building, Maria de Luna 3, Zaragoza, 50018, Spain (✉ dsamper@unizar.es, +34 876 55 56 10)

Abstract

This paper presents a method of correcting the effects caused by refraction phenomena in an optical measurement system. The correction algorithm proposed can be applied in many different photogrammetric applications affected by these effects. To validate this algorithm, a foot sole optical measurement system that uses several cameras to build a mesh of a foot sole has been used. This measurement system has six cameras that are protected by a safety glass that separates the cameras from the foot to be measured. The safety glass produces an air–glass–air interface that causes the refraction phenomena, producing deformations in the images. Due to the deformations it is impossible to obtain reliable metric information of the images captured using the measurement system. The developed correction algorithm is based on a grid layout and associated polynomials and makes it possible to correct the deformations and extract accurate metric information.

Keywords: refraction correction, photogrammetry, correction polynomials.

1. Introduction

The refraction phenomena caused by air–glass–air interfaces are the main source of error in camera calibration when the camera is encapsulated or protected by glass. They produce non-linear deformations in the images captured by the camera which do not have the mathematical collinearity on which several of the most frequently used camera calibration methods are based [1, 2]. Some of these methods are Tsai's method [3], Direct Linear Transformation (DLT) [4], and Faugeras' method [5]. In the case of refraction deformations, contrary to what occurs with other types of aberrations in images such as radial distortion, the modification that must be applied to a certain projected point on the image to remove this deformation does not depend exclusively on the image coordinates of the point [6]. For this reason, the classic techniques for distortion rectification on images are not valid for elimination of the aberrations caused by refraction phenomena.

The main techniques for eliminating the refraction effects have been developed in aerial and underwater photogrammetry applications. In the case of aerial photogrammetry the refraction phenomena are caused by the atmosphere. By contrast, in underwater applications, air–glass–water or air–water interfaces are inevitable due to the need to protect the camera from water or positioning the camera outside the water. These techniques can be separated into three groups: those that are based on camera systems with multiple views [7], methods using dual-plane calibration [6, 8], and theoretical model equations [9–11]. The two first

Article history: received on Apr. 29, 2013; accepted on Jul. 19, 2013; available online on Dec. 10, 2013; DOI: 10.2478/mms-2013-0051.

methods are commonly used in underwater applications, and model equations are used in both aerial and underwater photogrammetry. Techniques with multiple views are intended to be used in systems with encapsulated underwater cameras, in which the air–glass–water interface is usually perpendicular to the optical axis of the camera. Dual-plane techniques allow a greater range of positions and orientations of the cameras with respect to the interface, while model equations methods are based on polynomial equalities that attempt to represent mathematically the effects caused by the phenomenon of refraction. The latter method is a fairly inflexible approach that only gives good results in the applications for which the model equations were designed [9], and if there are subsequent changes in some of the applications' parameters, the results worsen significantly, especially in the case of variations in the distances between cameras and measured objects [12].

The present work discusses the method developed to correct the effect caused by refraction phenomena in a photogrammetric measurement system with the cameras protected by glass. The refraction rectification procedures developed so far focus mainly on underwater applications, such as swimming sports and marine life studies, in which the elimination of deformations is required but metrological accuracy is not necessary, although recently some authors have been getting close to millimeter accuracy using mathematical models in underwater applications [9]. The novelty of the correction method proposed, in comparison with those other methods, is that metrological accuracy can be achieved. To verify the validity of the method, several tests have been carried out in an optical measurement system that performs a three-dimensional (3D) reconstruction of the lower part of a foot sole from images taken by several cameras. The measurement made by the system is from the sole bottom to 10 mm in height. The system cameras are protected by glass that separates them from the foot to be measured, so there are two interfaces. An air–glass–foot interface appears in areas in which the foot is touching the glass surface, and in the zones where the foot is not in contact with the glass there is an air–glass–air interface. These interfaces make deformations appear in the images captured by the system due to the refraction phenomena. To correct these image deviations, an algorithm based on a grid layout with polynomials associated with each grid region has been used which bears certain similarities to the dual-plane calibration techniques that are used in underwater applications. The method proposed uses a grid to discretize the information previously obtained from the images by grey-scale techniques [13]. These kinds of grids are used in many vision-related applications, such as robot navigation [14], object positioning [15], and object tracking [16]. The discretization of the data by the grid may consist of two types of information extraction: extracting the information which coincides with the grid lines' intersections or extracting the information contained in the regions formed by the grid lines. The method shown in this paper uses this last type of discretization.

2. Refraction phenomena

The refraction phenomenon makes a wave change its direction and velocity when it crosses the interface between two media with different refractive indices. This only occurs when the wave passes between the two media at any angle other than 90° or 0°. Refraction causes the objects' projections in the images captured by an encapsulated camera to be deformed and displaced from their ideal positions. This image distortion increases with the angle between the incident ray in the camera sensor and a line through the camera optical center and it is perpendicular to the interface plane. From the point of view of the camera it is as though the objects captured by the camera were in fictitious positions with regard to their real positions.

3. Optical measurement system used in algorithm validation

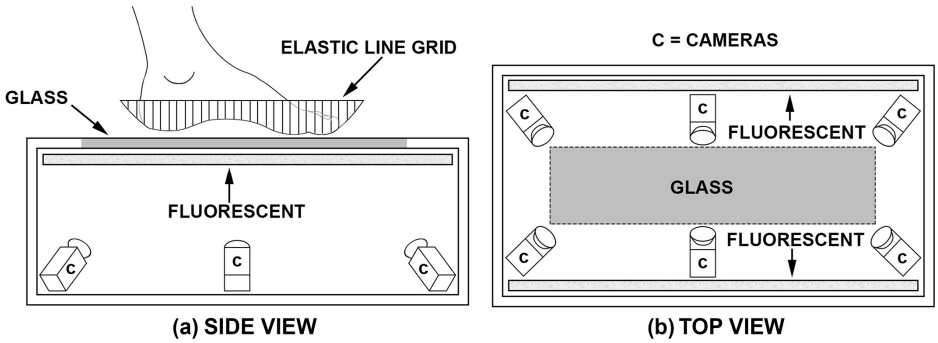

Fig. 1. a) Side view and b) top view of the measurement system.

The refraction correction method has been applied to a measurement system with six cameras (Fig. 1). Although in this case six cameras are used, the method can be used with any number of cameras, from only one to several. The system reconstructs a 3D mesh of 10 mm from the bottom of the sole (Fig. 2a) using the information extracted from images captured by the cameras (Fig. 2b). In these images an elastic line grid appears when it is deformed by the foot during its measurement. The projections of the lines of the elastic grid in the images allow construction of the 3D mesh using homographic techniques [9]. Because the sole is not symmetrical, the system cameras are not used symmetrically to reconstruct the mesh of the sole. The two cameras closer to the foot heel are used only to obtain information about this foot area, while the rest of the sole is reconstructed using the groups of three cameras on each side of the system. The area of the sole that is reconstructed by each of these camera groups is not symmetric either.

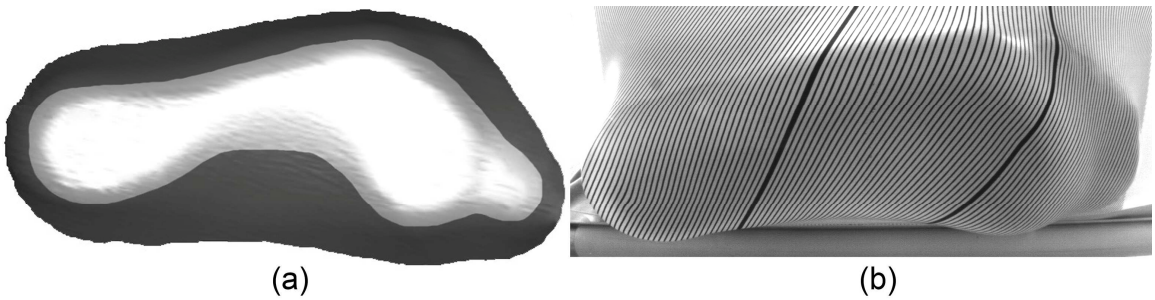

Fig. 2. a) Example of a sole as measured by the system. The light area corresponds to the useful measure of the lower part of the sole, from 0 to 10 mm. b) Example of an image captured by one of the cameras during the measurement process.

The line grid which supports the foot is separated from the cameras by a safety glass, 10 mm thick, on which the foot rests during the measurement process. Due to the presence of this glass there are two interfaces: the air–glass–air interface and the air–glass–foot interface, and consequently the images captured by the cameras are deformed and the metric information extracted is incorrect. Therefore, it is necessary to correct these image deformations in order to extract valid metric information.

The six system cameras are calibrated using the calibration method of Faugeras [5], which allows the 12 parameters of the projection matrix associated to each camera to be obtained. Also, a radial distortion correction model is used to correct the deviations caused by camera lenses. These calibrations are performed without removing the glass from the measurement system. Once the cameras have been calibrated the necessary parameters for correcting the

distortion caused by refraction are calculated. To calculate these adjustments the polynomials' parameters associated with the grid regions are used.

4. Correction model

Using the correction method proposed it is possible to obtain the parameters that allow the refraction deformation in the image coordinates (u,v) to be eliminated. To remove these shifts, a polynomial (1) that depends on the position of the displaced projected points in image coordinates (u,v) is used, and its result is the correction to be applied to the point to cause it occupy the position in which it would be located if there were no deformations in the images due to refraction. Each of these polynomials is associated with a particular region of the image, so it is necessary to apply a mesh to the image to be divided into regions and thus calculate the associated polynomials.

$$\delta = a + b{\cdot}u + c{\cdot}v + d{\cdot}u{\cdot}v + e{\cdot}u^2 + f{\cdot}v^2 + g{\cdot}u^2{\cdot}v^2 + \cdots , \tag{1}$$

Based on the above polynomial (1), several polynomials with different degrees of freedom were tested in order to check which the optimal ones are. For polynomials with three (2) and four (3) degrees of freedom the correction results obtained were not acceptable for this application, while for seven (4) or more degrees of freedom the results showed no significant improvements over the results obtained with six degrees of freedom (5). Finally a polynomial with six degrees of freedom (5) was chosen because it offered an optimal correction for the foot sole reconstruction.

$$\delta = a + b{\cdot}u + c{\cdot}v , \tag{2}$$

$$\delta = a + b{\cdot}u + c{\cdot}v + d{\cdot}u{\cdot}v , \tag{3}$$

$$\delta = a + b{\cdot}u + c{\cdot}v + d{\cdot}u{\cdot}v + e{\cdot}u^2 + f{\cdot}v^2 + g{\cdot}u^2{\cdot}v^2 + \cdots , \tag{4}$$

$$\delta = a + b{\cdot}u + c{\cdot}v + d{\cdot}u{\cdot}v + e{\cdot}u^2 + f{\cdot}v^2 . \tag{5}$$

In order to apply the correction, it is necessary to have the points affected by the deformation and the same points in their theoretical positions for the entire working area. The greater the density of data in the image work area, the better the results that are obtained with this method. As this correction only uses information of the points with and without deformation, it is completely independent of the interface which causes the refraction phenomena; that is, the correction is not dependent on the type of glass or its thickness, the index of refraction of the media, or the orientation of the measured object.

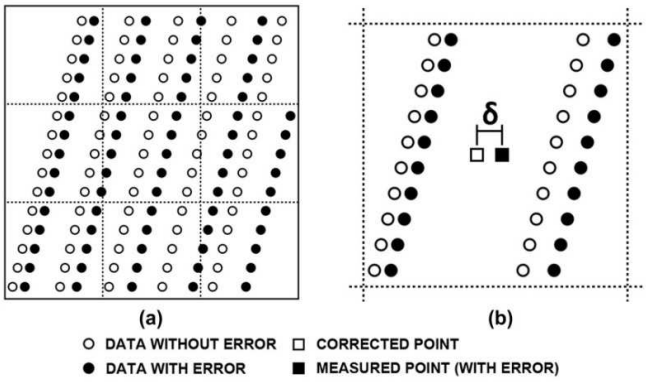

Fig. 3. a) Division into regions of the work area for the implementation of the correction method. b) The δ correction applied to any point within the region to eliminate displacement caused by the deformation of the image.

Data are divided into different regions by meshing the image work area. These data and regions depend on the characteristics of the optical measurement system to be corrected, especially on the number of cameras used. So, the data to consider in each region and the number and size of the regions will depend on the system functionality. For each of these regions, both displaced and non-displaced points (Fig. 3a) contained in each region are used to calculate the parameters of the associated polynomial. The calculation of the parameters is done by non-linear optimization, minimizing the difference between displaced points and non-displaced points. Once all the parameters of the polynomial associated with a given region have been calculated, it is possible to calculate the δ correction to be applied to any point in this region to remove the displacement caused by the image deformations (Fig. 3b).

5. Application of the correction method to the test measurement equipment

This section shows the procedure that has been followed to apply the correction to the test measurement system. The described procedure serves as an example of how to apply the proposed method to other measurement systems. To calculate the polynomials' parameters, a line template identical to the elastic line grid has been used. The pattern is formed by 200 lines which are contained in a plane, have an inclination of 45°, and are separated from each other by 2 mm. Although in this case a line template was used, any type of pattern with easily recognizable elements can be used, as it could be a regular array of n × m points. Firstly the template was placed in the measurement system, so that the entire template surface was in contact with the glass. When it was in its correct position, images were taken with each of the six system cameras (Fig. 4).

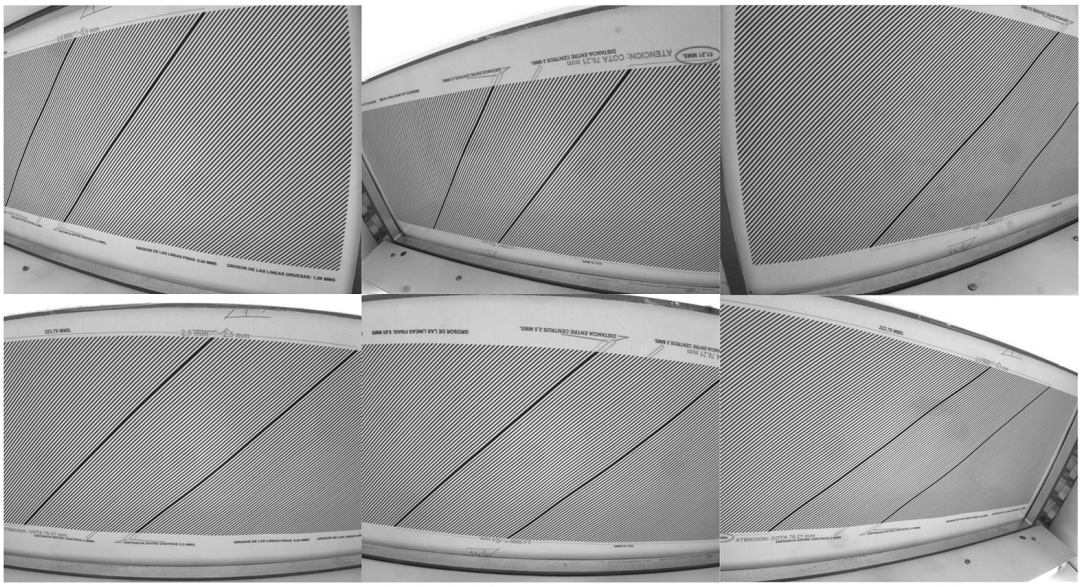

Fig. 4. Images of the line template captured by the six system cameras.

From the images captured, the coordinates of the pixels that form the template lines' projection on each image were extracted; for this purpose a technique based on the grey level gradient of the lines was used [9]. Only the lines that fall within the working area of each camera were extracted (Fig. 5).

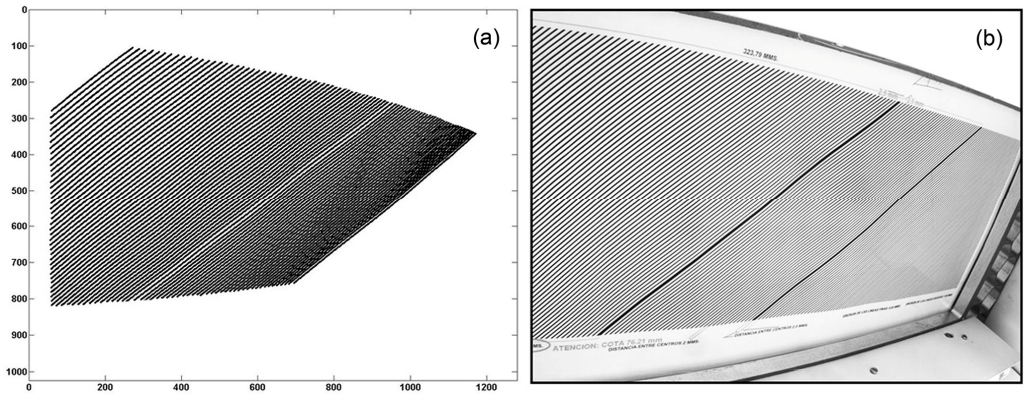

Fig. 5. a) Representation of the lines extracted from one of the images.
b) Image from which the lines were extracted.

Once the lines had been extracted, the lens radial distortion parameters obtained from the camera calibration were used to eliminate the deformation in the lines caused by this type of aberration. After that, data from the extracted lines of each camera were used to reconstruct, by homographic techniques [9], the plane containing the lines of the template measured with the system. With these homographic techniques the coordinates of the points that form the lines in the (X,Y,Z) world reference frame were calculated and used for building a stereolithography mesh (STL) representing the plane containing the reconstructed lines, and in Fig. 6 a top view of the reconstructed plane mesh can be seen.

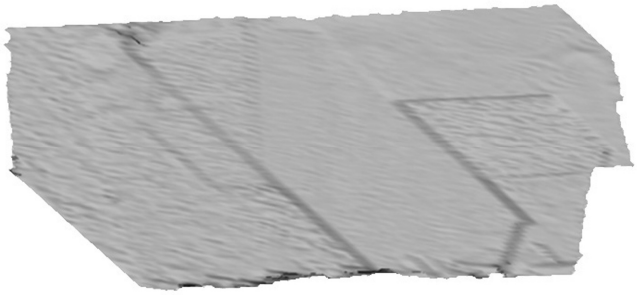

Fig. 6. Top view of the reconstructed plane using the data extracted from the images by homographic techniques.

As shown in Fig. 6, the reconstructed plane presents several jumps and irregularities that are not present in the line template plane. These irregularities are due to the construction of the plane that is made by merging three different point clouds. Each of these point clouds is built from metric information obtained by two or three system cameras, since each of the cameras is affected by the refraction phenomena in different ways due its position and orientation with respect to the glass. This circumstance and the use of the cameras described in Section 3 are the reasons why, on merging the reconstructed point clouds, jumps and irregularities appears in the final mesh of the reconstructed plane.

When comparing the merged point cloud used for building the STL with the ideal cloud that represents the line template plane it is possible to identify the errors made in the STL construction. Fig. 7 shows the maximum distance of the points from each of the reconstructed lines to their corresponding ideal lines.

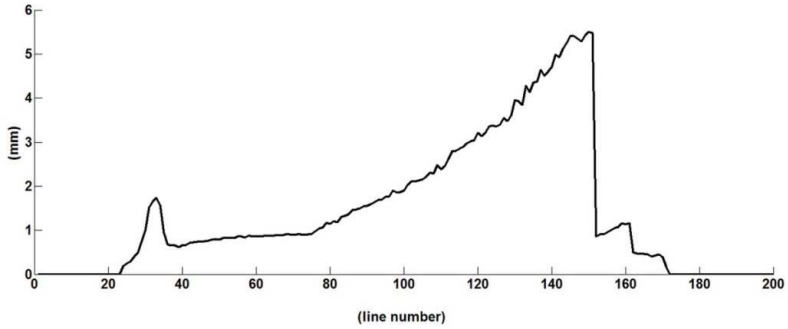

Fig. 7. Maximum distance for each of the template lines between the points belonging to a reconstructed line and its corresponding ideal line without deformation due to refraction.

As shown in the graph in Fig. 7, the maximum distance of the points from the reconstructed lines is up to 6 mm due to the effects caused by refraction in the images. This graph is not symmetric due to the use of different cameras during the measurement process. The first lines correspond to the heel area and are only measured by the two cameras that are closer to this area, while some areas of the rest of the sole are measured by the cameras that are furthest from these areas. Thus, when measured points are close to the camera the image deformation is smaller.

To calculate the correction model to be applied in the measurement system, it is necessary to know what the projection of the template lines in the image plane of each camera would be like if it were not affected by the refraction phenomena. To obtain the images from the template lines without deformation, the (X,Y,Z) coordinates of the points that make up the template lines and the cameras' calibration parameters have been used. With these data, six virtual images of the projected template lines were generated without refraction deformation or camera lens radial distortion. Each of these virtual images was paired with its corresponding real image, and the correction method was applied to each of these image pairs. These image pairs were divided into regions of 40 × 40 pixels, making an array of regions with a size of 25 rows and 31 columns.

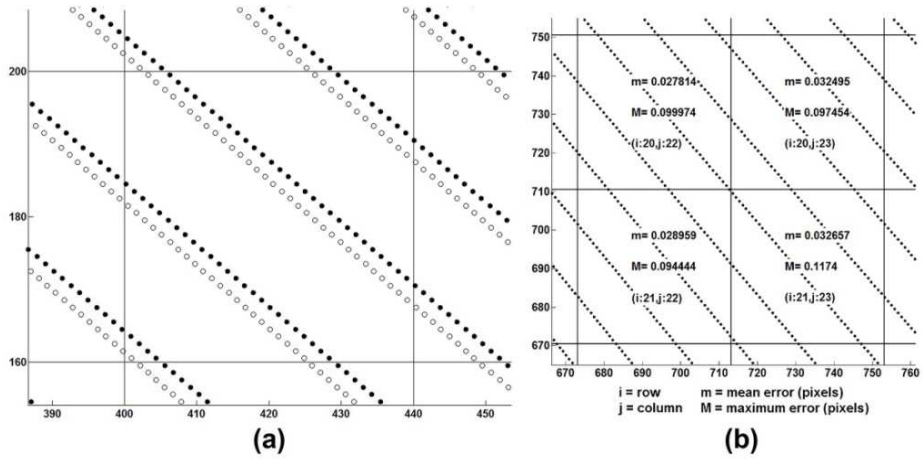

Fig. 8. a) One region in detail. Black points: lines affected by refraction deformation; white points: lines without refraction deformation. b) Results obtained in four regions after applying non-linear optimization to one of the images.

In Fig. 8a one of these regions can be observed in detail. The points corresponding to the lines affected by refraction (black points) and their homologous points belonging to the ideal lines without deformations (white points) can be seen.

The differences between the points affected by deformation and points without deformation are minimized by a non-linear optimization. As an example, the results of this optimization can be seen in Fig. 8b for four regions of one of the images, and in Table 1 the parameters obtained for the polynomials associated with these regions can be seen.

Table 1. Obtained parameters of the polynomials associated with the regions shown in Fig. 8.

	$\delta = a + b \cdot u + c \cdot v + d \cdot u \cdot v + e \cdot u^2 + f \cdot v^2$					
Region	**a**	**b**	**c**	**d**	**e**	**f**
(i:20,j:22)	–1.395e+02	2.079e-01	2.226e-01	–1.832e-04	–6.958e-05	–8.129e-05
(i:20,j:23)	2.774e+02	–6.413e-01	–1.693e-01	1.777e-04	3.800e-04	3.175e-05
(i:21,j:22)	1.346e+02	–3.219e-01	–7.459e-02	4.132e-06	2.386e-04	4.692e-05
(i:21,j:23)	–2.060e+02	2.603e-01	3.386e-01	–2.822e-04	–5.042e-05	–1.094e-04

Once the polynomials have been calculated for all the regions of each image, the STL of the template plane is reconstructed again, and as can be seen in Fig. 9 the jumps and irregularities shown in Fig. 6 are no longer observed.

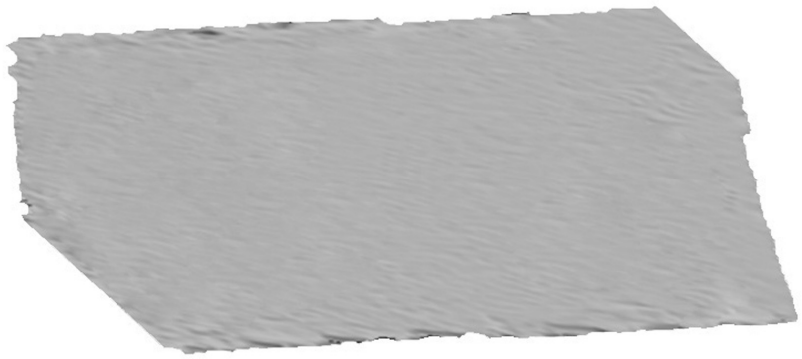

Fig. 9. Top view of the reconstructed plane using the data extracted from the images and homographic techniques after the correction of the refraction deformation.

If the maximum distances between the points of the lines forming the reconstructed plane and the points of the lines that form the ideal plane of the template are measured again after applying the correction, the maximum distances obtained do not exceed 0.16 mm (Fig. 10). From the comparison with errors of 6 mm obtained before correction of the refraction, it can be seen that these errors have decreased significantly. If the mean distances between the points of the reconstructed lines and the points of the lines of the ideal plane are calculated, the result obtained does not exceed 0.02 mm (Fig. 11).

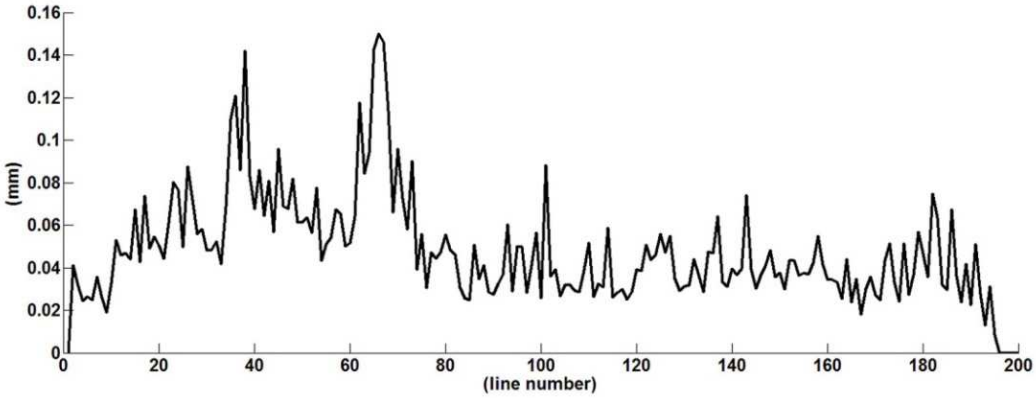

Fig. 10. Maximum distance for each of the template lines between the points belonging to a reconstructed line and its corresponding ideal line without deformation due to refraction after the refraction deformation has been corrected.

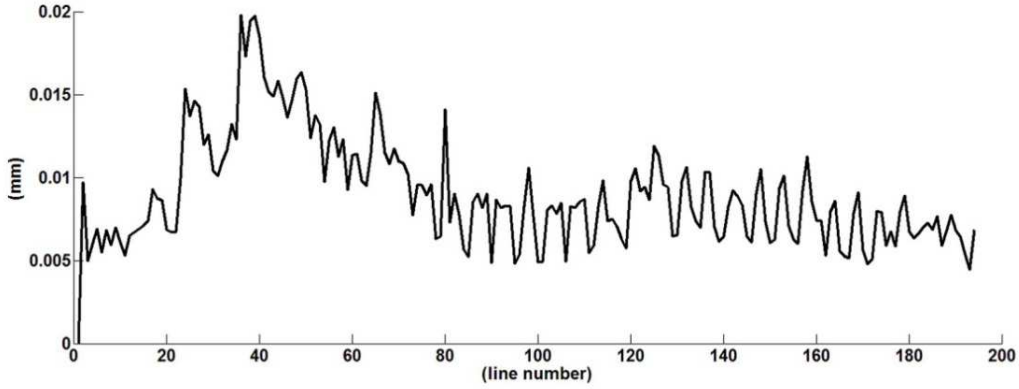

Fig. 11. Mean distance for each of the template lines between the points belonging to a reconstructed line and its corresponding ideal line without deformation due to refraction after the refraction deformation has been corrected.

Displacement caused by the refraction in the projection of a point in an image depends not only on the angle between the normal to the glass and the line formed by the point and the camera optical center but also on the distance between the observed point and the interface causing the refraction phenomena. In the case of the effects caused by radial distortion, all projected points that occupy the same position in an image have the same correction factor regardless of the distance between the observed point and the camera. This does not happen in the case of the deformation caused by the refraction, since projections from two different observed points that occupy the same position in an image may have different correction factors on the basis of their distances from the camera. The correction applied to the measurement system ensures that the deformation in the images is almost entirely corrected as long as the projected points in the image correspond to measured points that are in the same plane as the interface created by the system glass.

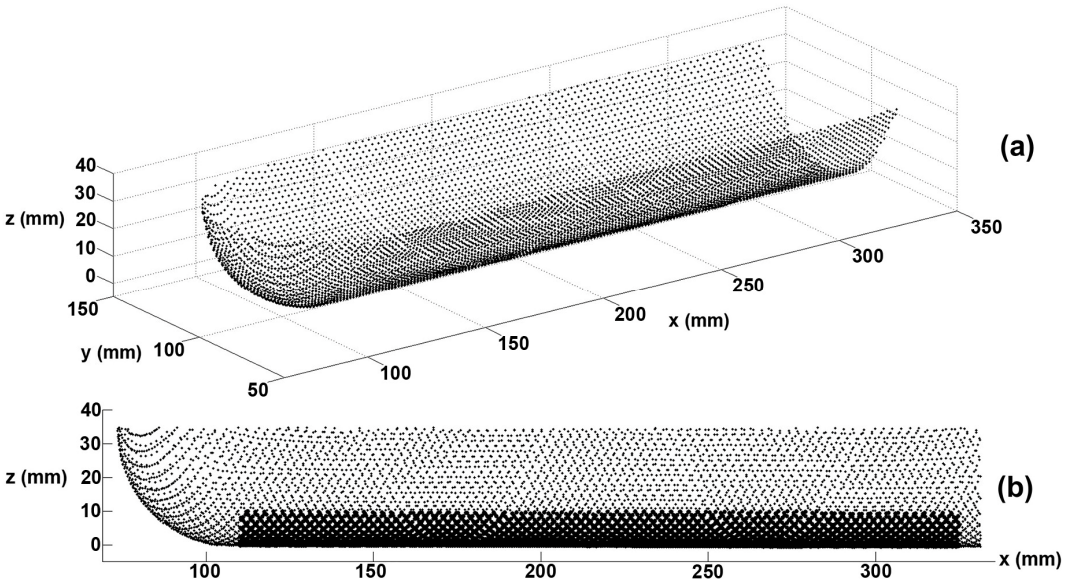

Fig. 12. a) Points cloud of the test object obtained from the images captured by the cameras. b) Bold points: control points used for calculating the error of the measurement equipment for points away from the glass.

The information to be measured with this equipment is not only provided by the surface of the elastic template that is in contact with glass. The equipment also obtains metric information from the surface that is not in contact with the glass. For this reason a test was performed to check how good the refraction correction is in the case of the points that are not in contact with the glass. In these tests an object with a cylindrical body and semi-spheres at its ends was used. The cylindrical body was measured with a coordinate measuring machine (CMM), and a radius of the cylindrical area of 34.54 mm and a form error of 0.05 mm were obtained. The test object was placed longitudinally in the elastic grid of the equipment so that the generatrix of the cylindrical zone was in contact with the glass. Finally a cloud of points (Fig. 12a) was obtained from the images captured by the measurement system.

To verify the quality of the correction for points away from the glass, the points of the reconstructed cloud of points whose Z coordinates were within the range of 0 mm to 10 mm and furthermore whose X coordinates were within the range of 110 mm to 325 mm (Fig. 12b) were used. Once these control points had been selected, they were grouped according to their Z coordinates, that is, according to their distance from the system glass. The distances between the measured points and the ideal surface of the test object obtained with the CMM were calculated, so the reconstruction error of the measurement equipment was obtained for points away from the glass (Table 2).

Table 2. Mean and maximum reconstruction errors according to the distance between the glass and the measured control points.

Range (mm)	**0 < Z < 1**	**1 < Z < 2**	**2 < Z 4**	**4 < Z < 6**	**6 < Z < 8**	**8 < Z < 10**
Mean error (mm)	0.033	0.047	0.056	0.065	0.073	0.081
Maximum error (mm)	0.158	0.184	0.205	0.213	0.228	0.244

In the case of the reconstructed points that are located at a distance of less than 1 mm from the glass, it can be observed that both the mean and the maximum reconstruction errors are similar to the results obtained in the reconstruction of the line template plane that was in

contact with the glass. As expected, the reconstruction error increases as the Z coordinate increases; that is, the error grows as the distance between the point and the glass increases.

Two reconstructions of the test object were made, one with refraction correction and another without this correction. It can be seen that the errors are greater when the correction method is not applied (Table 3). The absolute value of the difference between the actual radius of the test object and the radius of the reconstructed object is 0.240 mm without the correction and 0.028 mm when the correction is applied. In Table 3 the mean and maximum reconstruction errors in both cases can also be seen. As expected, the reconstruction errors are higher when the correction is not used to eliminate the refraction deformations from the images.

Table 3. Comparison of the radius of the test object and the mean and maximum reconstruction errors with and without the refraction correction.

Measurement	Test object radius (mm)	Mean error (mm)	Maximum error (mm)
Without correction	34.780	0.287	0.590
With correction	34.512	0.059	0.240

6. Conclusions

The correction algorithm developed that has been applied in the measurement system for sole 3D reconstruction successfully corrects the effects due to the refraction phenomena caused by the glass present on the measurement system. As seen in Section 5, the correction gets worse when reconstructing points away from the plane on which the correction polynomials have been calculated, in this case points with coordinate $z = 0$. According to the error specifications of the sole measurement system of a mean error in the reconstructed points lower than 0.1 mm, the worsening of the correction in the points away from the glass is perfectly acceptable. This result has been verified using the test object described in Section 5, due the difficulty in obtaining reliable measurements from a foot sole that could serve as a reference object. If in other applications it is necessary to obtain reliable metric information from points that are far away from the plane in which the correction is calculated, it will be necessary to calculate the correction polynomials using several correction planes at different distances from the glass. In this way, the correction parameters applied to points depend not only on the (u,v) coordinates where the points are projected to the image but also on the Z coordinate of the reconstructed point.

References

[1] Kunz, C., Singh, H. (2009). Hemispherical refraction and camera calibration in underwater vision. *Oceans'08 MTS/IEEE*, Kobe, Japan, 1–7.

[2] Kwon, Y.H., Lindley, S.L. (2001). Applicability of four localized-calibration methods in underwater motion analysis. *XVIII Int. Symp. Biomech. Sports*, Hong Kong, China.

[3] Tsai, R.Y. (1987). A versatile camera calibration technique for high-accuracy 3D machine vision metrology using off-the-shelf TV cameras and lenses. *IEEE J. Robot. Autom.*, 3(4), 323–344.

[4] Abdel-Aziz, Y.I., Karara, H.M. Direct linear transformation from comparator coordinates into object space coordinates in close-range photogrammetry. *Proc. Symp. Close-Range Photogramm.*, Falls Church, USA, 1–18.

[5] Faugeras, O. (1993). *Three-Dimensional Computer Vision: A Geometric Viewpoint*. Cambridge: MIT Press.

[6] Kwon, Y.H. (2000). A camera calibration algorithm for the underwater motion analysis. *Sci. Proc. XVII Int. Symp. Biomech. Sports*, Perth, Australia, 257–260.

[7] Treibitz, T., Schechner, Y.Y., Singh, H. (2008). Flat refractive geometry. *IEEE Trans. Pattern Recognit. Anal. Mach. Intell.*, 34(1), 23–28.

[8] Drenk, V., Hildebrand, F., Kindler, M., Kliche, D. (2000). A 3D video technique for analysis of swimming in a flume. *Sci. Proc. XVII Int. Symp. Biomech. Sports*, Perth, Australia, 361–364.

[9] Fan, Y., Huang, G., Qin, G., Chen, Z. (2012). Underwater photogrammetric theoretical equations and technique.*VII Int. Symp. Precis. Eng. Meas. Instrum.*, 832113.

[10] Georgopoulos, A., Agrafiotis, P. (2012). Documentation of a submerged monument using improved two media techniques. *18th Int. Conf. Virtual Systems and Multimedia*, 173–180.

[11] Murase, T., Tanaka, M., Tani, T., Miyashita, Y., Ohkawa, N., Ishiguro, S., Suzuki, Y., Kayanne, H., Yamano, H. (2008). A photogrammetric correction procedure for light refraction effects at a two-medium boundary. *Photogramm. Eng. Remote Sens.*, 74(9), 1129–1136.

[12] Telem, G., Filin, S., (2010). Photogrammetric modeling of underwater environments. *ISPRS J. Photogramm. Remote Sens.*, 65(5), 433–444.

[13] Aguilar, J.J., Lope, M., Torres, F., Blesa, A. (2005). Development of a stereo vision system for non-contact railway concrete sleepers measurement based in holographic optical elements. *Measurement*, 38(2), 154–165.

[14] Velat, J.S., Lee, J., Johnson, N., Crane, C.D. (2007). Vision based vehicle localization for autonomous navigation. *Int. Symp. Comp. Intell. Robot. Autom. CIRA2007*, Jacksonville, USA, 528–533.

[15] Lin, C.S., Chen, C.T., Wei, T.C., Chen, W.L., Chang, C.C. (2010). A positioning model of a two CCD camera coordinate system with an alternate-four-matrix look-up table algorithm. *Opt. Lasers Eng.*, 48(12), 1193–1199.

[16] Marcenaro, L., Vernazza, G., Regazzoni, C.S. (2002). Image stabilization algorithms for video-surveillance applications. *Int. Conf. Image Process.*, Thessaloniki, Greece, 7–10.